Stratigraphy and Nature of uranium mineralization from Precambrian Basement Granitoid – Srisailam Formation contact around Chitrial area, Cuddapah basin, Telangana

Summary

By

SNEHA MUKHERJEE
Registration No. – 14RS15210002

Supervisor:

Dr. Gautam Ghosh

Joint Supervisor:

Dr. Sankar Bose

1. Introduction

Continents are believed to grow by repeated accretion, collision and magmatic intraplating over the last 3.0 Ga of Earth's history (Polat *et al*., 1998; Santosh *et al*., 2015). The Neoarchean time represents a key period of continental crustal growth with major tectonic assembly and stabilization of large cratonic areas such as the Dharwar craton in India (Condie, 2000; Kroner *et al*., 2005). The Proterozoic Cuddapah Basin, developed along the eastern margin of the Dharwar craton exposes highly favourable lithostructural setup for uranium mineralization, especially in the northern part. A number of medium-grade and small- to medium-tonnage uranium deposits have been established at Lambapur, Peddagattu and Chitrial in the Srisailam Sub-basin and Koppunuru in the Palnad Sub-basin (Sinha *et al*., 1995, Verma *et al*., 2008) of the Cuddapah basin in recent times. These deposits are spatially concentrated along the contact between the basement granite and overlying sedimentary cover rocks of the Srisailam sub-basin. One such uranium prospect, the Chitrial outlier (Fig. 1) located along the north-west margin of the Srisailam sub-basin is the focus of the present study. The rocks of the Mesoproterozoic Srisailam Formation unconformably overlie the 2.2-2.4 Ga Palaeoproterozoic biotite rich basement granitoids of the East Dharwar Craton (Pandey *et al*., 1988) in the Chitrial area. The basement gneisses and granites of the East Dharwar Craton underwent a late Archaean transpression (Chadwick *et al*., 2000) during its oblique convergence with the West Dharwar Craton followed by extension and opening up of the Proterozoic Cuddapah basin in phases. Timing and genetic relationships of the vein-type uranium deposits with the host lithologies in the Chitrial area remains inconclusive till date. The present research programme encompasses results of a study on the petrogenesis of the

host granitoid rocks as well as on mode of occurrence, nature and distribution of the uraniferous mineralized zones in the host basement granitoids of the Chitrial area from collective field mineralogical, geochemical and geochronological studies (Table 1).

2. Geological Background

The Archaean crustal domain of southern India is classically termed as the 'Dharwar craton' which comprises of vast areas of TTG gneisses (regionally known as the Peninsular gneiss), two generations of volcano-sedimentary greenstone sequences (>3.0-Ga Sargur Group and 2.9-2.6-Ga Dharwar Supergroup) and late intrusive highly-potassic granite plutons (Jayananda *et al.*, 2006). The craton is commonly divided into two sub-blocks - the Western Dharwar Craton (WDC) and Eastern Dharwar Craton (EDC) based on the nature and abundance of greenstone belt rocks, degree of regional metamorphism, amount of partial melting as well as on nature and age of the surrounding basement. The Chitradurga greenstone belt situated in the western boundary of the *ca*. 2.518 Ga Closepet Granite (Naqvi and Rogers, 1987; Moyen *et al*., 2003) is generally considered as the dividing line between two cratonic blocks, WDC and EDC. The contact between WDC and EDC is not sharp, and there is a transition zone between Chitradurga shear zone and Closepet Granite. This boundary marks a drop in crustal thickness from 42–51 km in WDC to 34–39 km in EDC (Gupta *et al*., 2003). Vast amount of literature exists regarding the geology, structure, petrogenesis, geodynamic evolution and geochronology of the Dharwar Craton (Jayananda *et al*., 2000, 2013; Dey *et al*., 2012, 2014). The Dharwar craton is also important for its varied and sizable amounts of metal deposits like gold, copper, iron, uranium etc. In EDC uranium mineralization has been documented from Proterozoic Kaladgi Basin, and Cuddapah Basin (Sharma *et al*., 1995; Dhanaraju *et al*., 2002). The Cuddapah Basin has in recent times, gained additional importance because of discovery of several large uranium deposits from its

different parts. Genetically two types of uranium mineralization have been discovered from the Cuddapah basin.

1. Stratabound mineralization, in the dolomitic rocks of the Vempalle Formation and in the Pulivendla Formation (Sundaram *et al*., 1989) from the lower part of the Cuddapah sequence.
2. Structurally controlled vein-type deposits along basement-supracrustal contacts in the basin (Sharma *et al*., 1995). The occurrence of uranium mineralization is mainly confined to basement granites and to some extent in overlying sedimentary rocks along such contacts.

The Chitrial area is situated in the north-eastern fringe of EDC. In the Chitrial outlier, the *ca*. 1.7 Ga Mesoproterozoic Srisailam Formation (Collins *et al.,* 2015) nonconformably overlies the S-type granite basement with reported U-Pb zircon age of ca. 2.51-2.52 Ga (Mukherjee *et al*., 2017). U-mineralization occurs in close proximity to the unconformity surface between the granitic basement and the overlying undeformed sandstone (Verma *et al.*, 2009, Sinha *et al.,* 1995) of the Srisailam Formation. Significant surface radioactive anomalies, with values up to 0.177% U_3O_8 (n=9) along the basement granitoid – Srisailam Formation contact led to the establishment of a sizeable uranium deposit by Atomic Minerals Directorate (AMD) in recent years (Umamaheswar *et al*., 2009) from the Chitrial area. According to Verma *et al*. (2009), the Chitrial outlier can be sub-divided into five blocks according to decreasing U-enrichment, from the Main Block to the Block 4 (Fig. 1). Subsurface correlation sections reveal that the U-mineralization of the Chitrial area persists in grade and thickness along the nonconformable contact between the basement biotite granitoid and the overlying Srisailam Formation and continues over a strike length of 2 km.

These deposits have been the subject of intense research during the last couple of years in order to decipher the geological processes responsible for their formation (Rajaraman *et al.,* 2013). However, detailed geological data on mode of occurrence of uraniferous horizons, detailed geochemistry of uraniferous zones and their host granitoid rocks and geochronological dataset from different litho-sequences in the Chitrial area pin pointing the chronological events of the EDC. A lacuna also exists in understanding the role of deformation of basement granites vis-à-vis the covering sediments in facilitating fluid flow and uranium mineralization.

Objectives

1. Identifying the extent of development of the uraniferous zones and their relationships with the overlying and underlying lithounits in the study area.
2. Detailed petrographic studies for classification, characterization and identification of potential uraniferous zones and assessing their post-formational modifications, if any.
3. Geochemical analyses for characterizing tectonic set up and basement anomalies.
4. Geochronological studies for ascertaining chronostratigraphic evolutionary history of the terrain with special emphasis on timing of uranium mineralization and crustal growth.

3. Methodology

Whole-rock geochemical analyses for major and trace elements of the samples were carried out by X-ray fluorescence techniques using a Rigaku ZXS system equipped at Hiroshima University, Japan. (Kanazawa *et al*., 2001) Laser Ablation- Inductively Coupled Plasma Mass Spectrometer (LA-ICPMS) analysis using 213 nm Nd-YAG Laser (New Wave ResearchUP-213) coupled with Agilent 7500 ICP-MS was carried out on glass of the same powdered samples for trace elements and rare-earth element concentrations.

For geochronological analyses, the heavy minerals were separated using panning method under water. All the samples yielded variable number of zircon grains of different size population as well as different shape and colour. Microphotographs of the zircon grains were taken in back-scattered scanning electron microscope images (BSI) and cathodoluminescence (CL) images were taken using a JEOL JSM-7500F scanning electron microscope at Hiroshima University, Japan. For LA-ICPMS, zircon U-Pb isotope analysis of granite and sandstone were performed using 213 nm Nd-YAG Laser (New Wave Research UP-213) coupled with Agilent 7500 ICP-MS. Raw data were processed using the data reduction program Pepi-AGE (Dunkl *et al*., 2008). Common Pb was corrected using the formulation of Stacey and Kramers (1975). The processed data of both analytical procedures have been finally used for statistical plotting using Isoplot/Ex (Version 4.15; Ludwig, 2008).

Polished thin sections were examined for identifying mineralogy, paragenesis and textural relations of the ores using an optical microscope and scanning electron microprobe. Back Scatter Electron (BSE) imaging and preliminary semi-quantitative energy dispersive spectroscopic (EDS) analyses were carried out with the help of a TESCAN-Vega scanning electron microscope at the Presidency University, Kolkata, India.

Quantitative phase chemical analysis of uranium and pyrite were done using the JEOL JXA 8200 Electron Probe Microanalyzer (EPMA) at the Hiroshima University, Japan. The operating conditions were 15 kV accelerating voltage, 20 nA beam current and 1-2μm beam diameter. Natural standards were used in both instruments and raw data were corrected by the ZAF program.

4. The Study area: overview on different rock groups, contact relationships and structural elements

The main lithologies of the study area include the basement granitoids and the overlying sandstone-shale of the Srisailam Formation. The uraniferous horizons occur mostly within the basement rocks in sub-microscopic scale and are discussed in a separate section (Section 5.).

4.1 Basement granioids

Chitrial granites are medium to coarse-grained, pink and grey in colour. The contacts between the pink and grey granites are gradational (Fig. 2a). The granite is undeformed at most places and represents the massive variety which at places is represented by a porphyritic variety with elongated feldspar phenocrysts in cryptocrystalline quartzofeldspathic groundmass (Fig. 2b). These granites have been classified as A-type by Verma *et al*. (2008). However, discrete carbonaceous phases reported within granites (Latha *et al*., 2009) indicate low temperature and high pressure melting of sedimentary protolith. In the study area a suite of mafic enclave is found within the granites which are dominantly consisting of oriented biotite grains with minor muscovite and chlorite. These enclaves are devoid of chilled margin and possibly represent relics of older supracrustals present prior to the emplacement of the granite in the area. These mafic enclaves are stretched, elliptical and define a shape preferred orientation on plan which suggests syn-magmatic deformation (Fig. 2c). The massive granite is interspersed with small, isolated gneissic pockets (Fig. 2d) where the dominantly NW-SE trending gneissic foliation is defined by alternate quartzofeldspathic and biotite-rich layers. At places, the granites are affected by conjugate mesoscopic shear zone development and the massive to gneissic fabric changes to a mylonitic fabric (Fig. 2e). Basic dykes (*ca*. 1.4 - 1.3 Ga emplacement age) of three different orientations (trending N-S, WNW-ESE and ENE-WSW) traverse the granites around the Chitrial outlier (Murthy *et al*., 1987). Epidote, chlorite, pegmatite and quartz veins also traverse the granitic rocks in the region. The veins cut through the granites as well as the dykes and appear to mark the youngest intrusive event

within the basement granites. A late brittle deformation affected the basement granites and gneisses around Chitrial with development of shear and mixed-mode fractures (Fig. 2f) of variable orientations. Post-Srisailam faults trending N-S as well as WNW-ESE displace the outcrops at places and thus indicate large-scale late basement reactivation in the area in a later period. Intragranular and transgranular fracture sets are common in grain-scale while shear and mixed-mode fractures develop in outcrop-scale. Fracture density was measured by using 2m × 2m grids from all the mineralized blocks as conceived by AMD in the terrain. The measured data have been plotted in one histograms per block (Fig. 3). Comparing the histogram for every individual blocks it is concluded that the fracture density is highest in locations that fall within the Main Block of uranium mineralization. With increasing distances from the centre of the Main Block, the fracture density also shows a sharp decrease. The measured counts indicate that the average fracture density (35-50/m^2) measured at different locations in the 'Main Block' is much higher in comparison to that measured from the adjoining 'Block 1 & 2' (10 – 25/m^2) and 'Block 4' (10 – 15/m^2). Hence it can be concluded that the fracture density is inversely proportional with the distance from the centre of the Main Block. It indicates that the increased fracture volume in the basement rocks directly or indirectly controlled uranium ore concentration in the Chitrial area with the WNW-ESE to NW-SE fracture set playing an active role behind mineralization.

Under microscope granite suite is constituted of mostly massive rocks showing textures of magmatic crystallisation. Plagioclase occurs as zoned subhedral phenocrysts with scarce inclusions of biotite. K-feldspar phenocrysts have ragged outlines and contain inclusions of biotite and apatite. Muscovite occurs intergrown with, biotite. In places, biotite is associated with rutile, monazite and apatite where monazite is present along the grain boundaries and fractures in apatite. In gneissic variety, the foliation is mostly defined by elongated quartz-feldspar alternating with biotite ± chlorite flakes. In mylonites, the rocks

show evidence of extensive dynamic recrystallization and grain size fining. Where affected by later brittle fracturing, the rock has turned into chaotic breccia to cataclasites with angular clasts set in a fine grained matrix.

4.2 Srisailam Formation

The rocks of the overlying Srisailam Formation are mostly represented by thick quartzite units interspersed with shale and siltstone layers. Thin conglomerate and palaeosol horizons can be locally observed to have developed along the prominent unconformity surface present between the granite and the Srisailam Formation. The sedimentary rocks are largely undeformed and are sub-horizontal in attitude. These show effects of fracturing and brecciation locally where affected by faults and fractures of later generation.

Sandstone is the major rock type within the Srisailam Formation. This rock type occurs in huge abundance, occupying the uppermost portions of the topographic hills in the region. The sub-horizontal nature of the sandstone gives rise to the typical ‘MESSA’ type geomorphological features in the area. These are abound with primary sedimentary structures such as plane laminations, cross beddings and wave ripples of various geometries indicating deposition in shallow water wave-current dominated settings. Thin shale and siltstone horizons intersperse with thicker quartzite layers in the sequence.

Under microscope the quartzites show a comparatively simple mineralogy and can be identified as framework supported, medium to fine grained sub-feldspathic-arenites to quartz-arenites (Fig. 4a). Quartz is the dominant mineral varying between 95-98%, represented mostly by monocrystalline and polycrystalline varieties. The grains are anhedral to euhedral, mostly rounded to subrounded with few angular to sub-angular grains. Some of the feldspar grains show inclusion and corroded grain margins (Fig. 4b). These are represented by potash as well as sodic feldspar and are mostly altered. Interstitial clay minerals are present in some

thin sections. A red film of iron oxide is coated on most of the grains. An interlocking mosaic is developed due to silica overgrowth on the grains. Cementation is good and the grains cannot be easily disaggregated. The rock fragments are mainly of quartzite. Matrix comprises silica, muscovite, sericite, calcite and chlorite.

5. Ore mineralization

The Proterozoic basins all over the world gained much importance due to occurrence of high-grade uranium deposits (Sinha *et al*., 1995; Verma *et al*., 2008). Uranium mineralization is believed to be controlled by older basement structures that were reactivated and acted as channel ways for ore-bearing fluid circulation (Polito *et al*., 2004). In such cases, oxidizing and saline basinal fluid with U^{6+} ions interacts with reducing basement rocks (basement-hosted,) or reducing fluid from the basement (sediment-hosted) precipitates uranium as UO_2 (U^{4+}) at or near the unconformity surfaces (Kotzer and Kyser, 1995). In Chitrial area, imprints of mineralization are present both in basement and overlying sediments, but hosted mainly by the granite. Srisailam quartzite shows very low surface radioactive anomalies restricted to the silicified quartzite, in which the mineralization is disseminated and localized.

5.1 Textural evolution

The hydrothermal alteration associated with uranium mineralization consists of chloritization, hematitization, silicification and pyritization. The dominant U-bearing minerals are uraninite and coffinite that formed in several stages during the evolution. Fracture/veins within the granite are cemented by uraninite, coffinite, thorite, monazite, zircon, titanite, apatite and Fe sulphides. Uraninite and coffinite are predominantly associated with pyrite. Accessory minerals associated with U minerals include Ti-oxide, galena, zircon, biotite and hematite. Ti-oxides are generally associated with altered uraninite.

Disseminated pyrite presents within the basement along with chalcopyrite, sphalerite and associated chlorite, biotite and K-feldspar. Pyrite also occurs as euhedral grains along the vein or present as a rim around feldspar (Fig. 5a). Rounded to sub-rounded pyrite occurs also in association with Fe-Ti oxide. Magnetite present along the grain boundaries of hematite in association with coffinite and pyrite. Hematite also occurs surrounding chalcopyrite (Fig. 5b). Uranium mineralization is mainly restricted to the fractured granite. The fractures/veins within the granite are cemented by uraninite, coffinite and thorite (Fig. 5c). Uranium-bearing mineral also occur along the intergranular fractures of pyrite grain. Second generation vein pyrite is also observed which cuts the uranium-bearing mineral vein (Fig. 5d). Coffinite occurs in three principal textures, viz. (1) showing colloform texture (Fig. 5e), (2) mineralogically zoned fracture fill, and (3) alteration of uraninite (Fig. 5f). Uraninite changed to coffinite along the vein margin in presence of pyrite. Galena occurs as rim around pyrite (Fig. 5g) in the outer part of the vein, whereas the vein is composed of coffinite. Autunite, brannerite and uranophane (hexavalent uranium minerals) are also present in veins (Fig. 5h). Textural evidences suggest that these minerals resulted from oxidation of primary tetravalent uranium minerals and are, therefore, considered as secondary uranium minerals.

5.2 Phase chemistry

Pyrite: A total of 15 microprobe analyses were carried out on one sample of the basement granite. There are large variations in the concentrations of Co and Ni in pyrite. These variations correlate well with different modes of occurrences (e.g., disseminated vs. vein). Accordingly, compositional types of pyrite are classified based on their Co and Ni concentrations.

Type-A: Pyrite with high Co and no/low Ni.

Type-B: Pyrite with no/low Co.

Uraninite: A total of 27 microprobe analyses were carried out on one sample of the basement granite. Compositionally, the analyzed grains show variable contents of UO_2 (86.41−88.39 wt.%), and PbO (2.02−4.20 wt.%). ThO_2 content is very low (0 to 0.01 wt.%).

6. Geochemistry

Major, trace and REE geochemistry of the basement granite were done to understand the magmatic history of the host rock. Data reduction, recalculation and representation were done using the GCD-kit (Janoušek *et al.,* 2006).

6.1 Major element data

All the samples show SiO_2 variation (72.24–78.97 wt.%) and are characterized by high K_2O (4.18 –7.31 wt.%) contents. Although the samples plot in the granite field in the normative Ab-An-Or diagram, they plot in the monzogranite field in the QAP diagram (Fig. 6a). Sample CT31, however, plots within the alkali feldspar-granite field. These rocks show peraluminous character with A/CNK values 1.0-1.6. This is also vindicated by their plots within the diagram of Frost *et al*. (2001) (Fig. 6b).

6.2 Trace element data

Trace element compositions of the samples show variations in terms of Sr (22 – 276 ppm) and Ba (222 – 974 ppm). Zr concentration is moderate in all the samples (146-249 ppm). All the samples contain moderate Rb and Y with high La/Nb (3.59-6.71) and low Ce/Pb (1.21-2.81) ratios. Plots of Zr vs. Ga/Al, FeOt vs. Ga/Al, Y vs. Ga/Al, Zn vs. Ga/Al, and Zn vs. Ga/Al show that the samples plot under I, S and M - type fields (Whalen, 1987) (Fig. 6c). Tectonic discrimination diagrams with Rb vs. (Y+Nb), Nb vs. Y, Rb vs. (Ta+Yb) and Ta vs.

Yb show that all the samples plot in the boundary between syn-collisional and volcanic arc granites (Pearce et al., 1984; Fig. 6d).

6.3 REE data

Chondrite-normalized REE patterns of the samples (Boynton, 1984) are distinctly enriched in character and more fractionated for LREE compared to the HREE with negative Eu anomalies (Eu/Eu*=0.35-0.88) (Fig. 6e) Primordial mantle-normalized plots (Taylor and McLennan, 1995) show distinct enrichment of LILE (especially Rb, U, Th, La, and Ce) and prominent Ba, Sr, Nb, and P anomalies (Fig. 6f). U content is somewhat high in sample CT 31. Samples represent more or less similar character with strong (Eu/Eu*=0.30-0.55) to moderate (Eu/Eu*=0.76) negative Eu anomalies.

7. Geochronology

A detailed zircon U-Pb geochronological analysis of the granitic rocks and the cover rocks from Chitrial outlier were carried out to understand the emplacement age of granite as well as the detrital ages of overlying sandstone.

7.1Geochronology of basement granite

Selective six samples (CT 206, CT 31, CT 65, CT 207, CT220, CT210) comprising of granite gneiss and granite, were analyzed using LA-ICP-MS and data reduction, recalculation and representation were done using the Isoplot (Ludwig, 2008).

Zircon grains from the granite gneiss CT 206 yield a group age of 2524±35 Ma (2σ, MSWD = 6.6, confidence = 95%; Fig. 7a). Probability density plot shows Minor age peaks of *ca*. 2465 Ma, *ca*. 2575 and *ca*. 2625 Ma. One spot from the core yields near-concordant date of 3000±30Ma. Sample CT 31represents the group age of 2524±10 Ma (n=29, MSWD = 2.3;

Fig. 7b). Two spots from the cores region shows older age of 3567±39 Ma and 3000±34 Ma. In the $^{207}Pb/^{206}Pb$ probability density diagram, minor peaks at ca. 2955 Ma and ca. 3406 Ma are also indicated. In sample CT 65 dates from the overgrowth domain yields group age of 2525±24 Ma (MSWD = 2.2, confidence = 95%; Fig. 7c). Probability density plot show a sharp peak of ca. 2525 Ma. Two near-concordant spots from the core yield dates of 3824±35 Ma and 3200±23 Ma. CT 207 show a group age of 2514±10 Ma (n =9, MSWD = 0.83; Fig. 7d). Probability density plot shows minor peaks of *ca*. 2455 Ma, *ca*. 2600 Ma and *ca*. 2680 Ma. One spot from the core yields much older discordant date of 3120±37 Ma. Zircon grains of sample CT 220 show a highly scattered distribution (Fig. 7e). One discordant spot (discordance 13.2%) from the core yield 3811±41 Ma date while another near-concordant spot yield 2843±33 Ma date. In CT 210, two older, concordant data from the core yield spot ages of 2706±28 Ma and 2648±28 Ma. Sixteen near-concordant (< 5% discordance) dates from the overgrowth yield a weighted average of mean $^{207}Pb/^{206}Pb$ ages of 2519±16 Ma (n=14, MSWD = 3.2; Fig. 7f). So, all the samples collected from Chitrial area represent more or less similar weighted mean age of the analysed zircon grains.

In summary, pooled ages from the analyzed samples (except sample CT220) show `correlated with the formation of the oscillatory-zoned zircon with or without inherited cores. This is therefore the age of crystallization of the Chitrial granite suite. Interestingly, zircons from all the samples show strong discordance, specifically from the disturbed oscillatory zoned domains. This is possibly related to isotopic disturbance during a much younger event, or it may cause due to the variable uranium contents of the measured zircon grains. However, the lower age intercept is difficult to constrain as there is no near-concordant data showing younger age. Thus, this discordance is may be related with much younger uranium mineralization event.

7.2 Geochronology of cover rocks:

Diagnostic detrital zircon age peaks that occur at 2520 Ma, 3000 Ma and 3200 Ma correspond to established ages of the Precambrian basement rocks and suites of granitic plutons associated with the EDC in Chitrial area. Detrital zircon geochronology data from the sediments around Chitrial show that the dominant group of zircon have group age of 2468±18 Ma to 2520±19 Ma (Fig. 8a). Younger dates are discordant without any proper lower intercept ages in the concordia plots. Older zircon cores with spot data ranging from 2636±28 Ma to 3200±7 Ma (Fig. 8b) are interpreted as grains inherited from the crustal source region or from the wall-rock of the granite intrusion. From the detrital zircon data it can be inferred that source of the sediments is proximal.

8. Discussion

8.1. Petrogenesis of Neoarchean granite

Samples of the Chitrial granite suite show variable SiO_2 (72.24–78.97 wt.%) and high K_2O (4.18 –7.31 wt%) contents. All the samples are Sr-poor, and low to moderate Sr/Y (1.2 – 26.1) ratio indicates low-pressure melting condition of the source. With normative corundum (0.83-2.12) and presence of both biotite and muscovite are indicative of S-type character. Rb/(Y+Nb) and Nb/Y plots indicate syn-collisional to volcanic arc tectonic setting, characteristics of orogenic S-type granites (Pearce *et al*., 1984; Fig. 6d). So, all the evidences converge towards the fact that Chitrial granite suite is compositionally S-type.

High La/Nb and low Ce/Pb ratios and negative Nb anomalies of all the samples are characteristics of convergent margin magmas (Rudnick, 1995). The Nb-anomaly is probably inherited from the magma source, and clearly reflects a subduction-related geochemical signature of the source (El Baghdadi *et al*., 2003). Negative Sr anomaly possibly implies plagioclase fractionation. Therefore, the evolved geochemical composition resembles the

granite composition produced by typical intracrustal melting of Archaean sediments (Beakhouse and McNutt, 1991). Since the granites show broadly S-type characters, these could have been generated due to melting of metasediments of the middle crust (Kemp *et al*., 2007).

In Indian perspective, the *ca*. 2.50 Ga granitic plutonism and crust formation far outweigh the *ca.* 2.70 Ga global event. It is important to note that the southern Indian crustal block and in particular the EDC witnessed widespread granitic activity in late Neoarchaean (*ca.* 2.56-2.51 Ga; Jayananda *et al*., 2013). Thus, the southern and central Indian crustal blocks characterized by amalgamated proto-continents, mostly formed and stabilized by large scale granite magmatism in late Neoarchaean (*ca*. 2.51-2.50 Ga; Meert *et al*., 2010). Geochronological data from the granites around Chitrial in north-eastern EDC show that the dominant group of zircon are of crystallization age 2514±10 Ma to 2525±24 Ma. Older zircon cores with spot data ranging from 2706±28 Ma to 3824±35 Ma are interpreted as grains inherited from the crustal source region or from the wall-rock of the granite intrusion. The crystallization age determined from zircon from Chitrial area is similar to 2523±39 Ma granite in the nearby Kadiri belt of EDC (Dey *et al*., 2014). Therefore, the granites from Chitrial area was possibly a part of the extensive granite suite that was emplaced in pulses during the span of *ca*. 2.53-2.51 Ga attesting significant addition of juvenile crust to the entire southern Indian crustal block in end Neoarchaean.

8.2. Ore mineralization

Pyrite, chalcopyrite, sphalerite and galena are the sulphide bearing minerals, in which the pyrite is the predominant one constituting about 90% of the total sulphide minerals. These minerals occur in various forms and textures (Craig 2001). Sulphides acted as the prime reductants for the precipitation of uranium (Pandit *et al.*, 2002). Studies have been done on

two generations compositionally and texturally different pyrite. The uranium minerals containing tetravalent uranium less abundant and include uraninite, coffinite and uranothorite. All of the known occurrences of these tetravalent uranium minerals indicate that deposition took place in a primary reducing environment mainly governed by deposition of disseminated or framboidal pyrite, chalcopyrite and sphalerite. Trace amount of secondary hexavalent U-minerals, formed during supergene leaching, are also present. Based on cross-cutting relationships and textures observed in thin section, the paragenetic history of the deposit can be divided into seven stages (Fig. 9). The total mineralization is divided into two fluid regimes.

Reducing condition: It involves the evolution of stage I to stage V minerals. The earliest hydrothermal phases, consisting of disseminated or framboidal pyrite, chalcopyrite and sphalerite, indicate pre-ore stage assemblages which governed a reducing environment. Magnetite formed in this environment, by the reduction of hematite. Uranium bearing highly oxidized hydrothermal fluid which contained U^{6+} was reduced to U^{4+} and precipitates as uraninite in this reducing environment where pyrite acted as reductant (Jefferson *et al*., 2007). Experimental/natural data suggest that hydrothermal uraninites formed at temperatures as high as 300-500°C which is in the stability field of UO_{2+x} (Alexandre and Kyser 2005). Therefore, it is reasonable to expect that uraninite precipitated as a complex U^{4+} and U^{6+}-oxide at this temperature range. A pyrite vein followed by the u-bearing mineral vein is also noticed which act as reductant in the formation of coffinite from uraninite. Coffinite can form from silica-rich aqueous solutions in contact with dissolved uranium species in a reducing environment at generally low temperature (Min *et al*., 2005).

Oxidizing condition: It includes stage VI and stage VII minerals. Replacement of uraninite by coffinite is another process that leads to Pb release from uraninite (Janeczek and Ewing, 1992). Substitution of Pb by Si in uraninites is indicative of alteration. By this process, Pb

was preferentially removed from uraninite, and the uraninite was gradually replaced by Si-rich material. A uniform distribution of removed Pb and crystallization of galena outside of pyrite in the presence of uraninite and coffinite grains suggest an oxidizing environment (Janeczek and Ewing, 1995). Under this oxidizing environment U^{4+} was oxidized to U^{6+} to form secondary uranium minerals like brannerite, autonite and uranophane.

Chitrial uranium deposits has already been identified as unconformity-associated uranium deposits (Sinha *et al*., 1995), but the mineralization in the Chitrial area is mainly indicated by uraninite vein and the occurrence of alteration product is restricted in intergranular and intragranular fracture within basement granite. The dominant sulphide is pyrite which is a character of vein type deposits (Cathelineau, 1981). ThO_2 wt% in uraninite vary from 0.001 to 0.018 i.e less than 0.3 wt.% which is a typical character of vein type deposits (Alexandre *et al*., 2016). Hydrothermal signatures in the form of bleeding pyrite in the granite of Chitrial area are reported by Verma *et al*. (2009). According to Alexandre *et al*. (2016), despite the variability of these deposits, their formation involves transportation of U by oxidizing fluids, which is the only possible explanation for the negligible amounts of Th in their uraninites. Lindgren (1933) defined the 'vein-type deposit' as sheet-like masses of minerals occupying or following a fracture or a set of fractures in the enclosing rock. So, Fractures play an important role either as direct pathways for ore-bearing fluids or channels for circulation of basinal brines that eventually concentrate the ore minerals scavenging the host basement near the deposition surfaces in vein type deposits which is a typical feature of Chitrial uranium deposits. Establishment of a near one-to-one relationship between increase in rock-fracture volume and the Chitrial uranium deposit becomes significant in this respect. So, Uranium-mineralization in Chitrial area may represent a hydrothermal vein type deposits. Hydrothermal fluid with the highest temperature up to 350 °C (Alexandre *et al*., 2016) may

be responsible for hydrothermal solutions driven by magmatism-tectonism along the fault and fracture zone of host-granite.

8.3. Geodynamic Model of basement granites and Chronological Sequence:

Several models (arc accretion, mantle plume, combined accretion-mantle plume and hot orogen) have been proposed to explain the complex geodynamic evolution of EDC-WDC during the Late Archean time (Peucat *et al*., 2013). In view of the existing ideas, the present work proposes that the subduction-related slab of EDC underwent partial melting at the end of the Late Archean time (*ca*. 2.52-2.51 Ga) and brought the magma to shallower level through deep shear zone and fault system. The syn-kinematic monzogranites were produced by intracrustal melting where melting was caused by the deep burial of clastic sediments (Fig. 10) and subsequent incubational heating of the crust which implies that crustal recycling played an important role in the long-term stabilization of continental crust as envisaged by many workers (Dey *et al*., 2012).

The earlier reported Rb-Sr whole rock age of the granite basement of the Chitrial area was *ca*. 2.40-2.20 Ga (Pandey *et al*., 1988). The new findings in the present work based on U-Pb zircon, however modifies the age of the basement granite to be *ca*. 2.51-2.52 Ga (Mukherjee *et al*., 2017) which is older than the earlier Rb-Sr age of the granites (Pandey *et al*., 1988). This is in tune with similar Neoarchaean granitoid ages reported from other parts of EDC (Dey *et al*., 2014) supporting the earlier contention that the EDC evolved through extensive granite plutonism in end-Archaean. The reported age of the Mesoproterozoic Srisailam Formation at present is *ca*. 1.7 Ga (Collins *et al*., 2015). However, the presently obtained U-Pb zircon ages from overlying sediments of the Srisailam Formation yield maximum depositional age of the sediments as *ca*. 2468-2488 Ma. As the later age is obtained from two samples collected from the basal part of the sequence, the age might

indicate the age of the nearby basement rocks which mostly acted as the source for the overlying sediments. The *ca*. 1700 Ma depositional age of the Srisailam Formation according to Collins *et al*. (2015) needs to evaluated using further analysis of samples from higher up in the stratigraphic sequence of the Srisailam Formation. The latter comprises basal pebbly to gritty quartzite which grades upward to a thick quartzite showing intercalation with dark grey shale and feldspathic quartzite. Somewhere the boundary line between the basement granite and the overlying sediments are marked by paleosole deposits. Uranium ore mineralization is also common in overlying Srisailam sediments which is documented from Peddagattu and Lambapur sub-basin (Thomas *et al.,* 2014). Therefore, both the basement and cover rocks were affected by uranium-rich fluid which implies that the mineralization event is younger than the cover rock formation. The ore-forming fluids were likely derived from remobilization of pre-existing U-rich basement rocks, and ascended upward along deep fracture systems that resulted from brittle reactivation of early ductile shear zones (Table 2).

9. Conclusion

- Chitrial outlier is a part of the EDC and composed mainly of granite with overlying sandstone of the Srisailam Formation. These rock units are separated by nonconformity.
- The granitic basement of the Chitrial outlier show ‘S’ type geochemical characters.
- U-Pb zircon data suggest crystallization age of the granite suite between 2514±10 Ma and 2525±24 Ma.
- Detrital zircon data from the Srisailam sandstone show that the dominant zircon group age of 2468±18 Ma and 2488±19 Ma. This implies the sediment was sourced from proximity, possibly from the underlying granite.

- Uranium mineralization in the basement granite and the overlying sandtone was controlled by oxygen fugacity in the ore-bearing hydrothermal fluid. This mineralization could be related with the later stage fracture reactivation of EDC during a major younger tectonic activity.

Funding

A part of this dissertation was carried out from the funding of Board of Research in Nuclear Science (BRNS), Department of Atomic Energy (DAE), Government of India (Proposal number (Project No. : 2011/36/59-BRNS/2186)

References

Alexandre, P. and Kyser, T.K., 2005**.** Effects of cationic substitutions and alteration in uraninite, and implications for the dating of uranium deposits. The Canadian Mineralogist, **43(3)**, 1005-1017.

Alexandre, P., Kyser, K., Polito, P. and Thomas, D., 2016**.** Alteration mineralogy and stable isotope geochemistry of Paleoproterozoic basement-hosted unconformity-type uranium deposits in the Athabasca Basin, Canada. Economic Geology, **100(8)**, 1547-1563.

Beakhouse, G.P., McNutt, R.H. 1991. Contrasting types of Late Archean plutonic rocks in northwestern Ontario: implications for crustal evolution in the Superior Province. Precambrian Research 49, 141-165.

Boynton, W.V. 1984. Cosmochemistry of the rare earth elements: Meteorite studies, in Henderson, P. (Ed.), Rare earth element geochemistry: Amsterdam, Elsevier 63–107.

Cathelineau, M., 1981. Les gisements uranifères de la presqu'île guérandaise (Sud Bretagne); Approche structurale et metallogénique. Mineralium Deposita, 16(2), 227-240.

Chadwick, B., Vasudev, V.N., Hegde, G.V. 2000. The Dharwar craton, southern India, interpreted as the result of Late Archaean oblique convergence. Precambrian Research 99, 91–111.

Collins, A.S., Patranabis-Deb, S., Alexander, E., Bertram, C.N., Falster, G.M., Gore, R.J., Mackintosh, J., Dhang, P.C., Saha, D., Payne, J.L., Jourdan, F. 2015. Detrital mineral age, radiogenic isotopic stratigraphy and tectonic significance of the Cuddapah Basin, India. Gondwana Research 28, 1294-1309.

Condie, K.C. 2000. Episodic continental growth models: afterthoughts and extensions. Tectonophysics 322, 153-162.

Craig, J.R., 2001. Ore-mineral textures and the tales they tell. The Canadian Mineralogist, 39(4), 937-956.

Dey, S., Pandey, U.K., Rai, A.K., Chaki, A. 2012. Geochemical and Nd isotope constraints on petrogenesis of granitoids from NW part of the eastern Dharwar craton: possible implications for late Archaean crustal accretion. Journal of Asian Earth Science 45, 40-56.

Dey, S., Nandy, J., Choudhary, A.K., Liu, Y., Zong, K. 2014. Origin and evolution of granitoids associated with the Kadiri greenstone belt, eastern Dharwar craton: A history of orogenic to anorogenic magmatism. Precambrian Research 246, 64-90.

Dhanaraju, R., Kumar, M.K., Babu, E.V.S.S.K., Pandit, S.A. 2002. Uranium mineralization in the Neoproterozoic Bhima Basin at Gogoi and near Ukinal:An ore petrological study. Jour.Geol.Soc.India, 59, 299-322.

Dunkl, I., Mikes, T., Simon, K., von Eynatten, H. 2008. Brief introduction to the Windows program Pepita: data visualization, and reduction, outlier rejection, calculation of trace element ratios and concentrations from LAICPMS data. Mineralogical Association of Canada, Short Course 40, 334-340.

El Baghdadi, M., El Boukhari, A., Jouider, A., Benyoucef, A., Nadem, S. 2003. Calc-alkaline arc I-type granitoid associated with S-type granite in the Pan-African Belt of Eastern Anti-Atlas (Saghro and Ougnat, South Morocco). Gondwana Research 6, 557-572.

Frost, B.R., Barnes, C.G., Collins, W.J., Arculus, R.J., Ellis, D.J., Frost, C.D. 2001. A geochemical classification for granitic rocks. Journal of Petrology 42, 2033-2048.

Gupta, S., Rai, S.S., Prakasam, K.S., Srinagesh, D., Bansal, B.K., Chadha, R.K., Priestley, K., Gaur, V.K. 2003. The nature of the crust in southern India: implications for Precambrian crustal evolution. Geophysical Research Letters 30, 1419, doi:10.1029/2002GL016770, 8.

Janeczek, J. and Ewing, R.C., 1992. Structural formula of uraninite. Journal of Nuclear Materials, 190, 128-132.

Janoušek, V., Farrow, C. M., Erban, V. 2006. Interpretation of whole-rock geochemical data in igneous geochemistry: introducing Geochemical Data Toolkit (GCDkit). Journal of Petrology 47, 1255-1259.

Jayananda, M., Moyen, J.-F., Martin, H., Peucat, J.-J., Auvray, B., Mahabaleshwar, B. 2000. Late Archean (2550–2520 Ma) juvenile magmatism in the Eastern Dharwar Craton, Southern India: constrains from geochronology, Nd–Sr isotopes and whole rock geochemistry. Precambrian Research 99, 225–254.

Jayananda, M., Chardon, D., Peucat, J.-J., Capdevila, R., Martin, H. 2006. 2.61 potassic granites and crustal reworking, western Dharwar craton (India): tectonic, geochronologic and geochemical constraints. Precambrian Research 150, 1–26.

Jayananda, M., Tsutsumi, Y., Miyazaki, T., Gireesh, R.V., Kapfo, K.U., Hidaka, H., Kano, T. 2013. Geochronological constraints on Meso-and Neoarchean regional metamorphism and magmatism in the Dharwar craton, southern India. Journal of Asian Earth Science 78, 18-38.

Jefferson C.W., Thomas D.J., Gandhi S.S., Ramaekers P., Delaney G., Brisbin D., Cutts C., Quirt D., Portella P., and Olson R.A., 2007. Unconformity associated uranium deposits of the Athabasca Basin, Saskatchewan and Alberta, in Goodfellow W.D. Ed., Mineral Deposits of Canada: A Synthesis of Major Deposit-Types, District Metallogeny, the Evolution of Geological Provinces, and Exploration Methods: Geological Association of Canada, Mineral Deposits Division, Special Publication No. 5, 273-305

Kanazawa, T., Sager, W.W., Escuita, C. 2001. Explanatory notes. Proceedings of the Ocean Drilling Program, Initial Report 191, p. 46.

Kemp, A.I.S., Hawkesworth, C.J., Foster, G.L., Paterson, B.A., Woodhead, J.D., Hergt, J.M., Gray, C.M., Whitehouse, M.J. 2007. Magmatic and crustal differentiation history of granitic rocks from Hf-O isotopes in zircon. Science 315, 980-983.

Kotzer, T.G. and Kyser, T.K., 1995. Petrogenesis of the Proterozoic Athabasca Basin, northern Saskatchewan, Canada, and its relation to diagenesis, hydrothermal uranium mineralization and paleohydrogeology. Chemical Geology, 120, 45-89.

Kröner, A., Wilde, S.A., Li, J.H, Wang, K.Y. 2005. Age and evolution of a late Archean to Paleoproterozoic upper to lower crustal section in the Wutaishan/Hengshan/Fuping terrain of northern China. Journal of Asian Earth Science 24, 577-595.

Latha, A., Nagendra Babu, G., Som, A., Umamaheswar, K., Maithani, P.B. 2009. First reported occurrence of carbonaceous matter in Chitrial Granite and its implications. International Journal of Earth Sciences and Engineering 4, 272-276.

Lindgren, W. 1933. Mineral deposits. Fourth Ed.

Ludwig, K. 2008. Manual for Isoplot 3.7: Berkeley Geochronology Center Special Publication No. 4, rev. August, 26, p.77.

Meert, J.G., Pandit, M.K., Pradhan, V.R., Banks, J., Sirianni, R., Stroud, M., Newstead, B., Gifford, J. 2010. Precambrian crustal evolution of Peninsular India: a 3.0 billion year odyssey. Journal of Asian Earth Science 39, 483-515.

Min, M., Chen, J., Wang, J., Wei, G. and Fayek, M., 2005. Mineral paragenesis and textures associated with sandstone-hosted roll-front uranium deposits, NW China. Ore Geology Reviews, 26(1-2), 51-69.

Moyen, J.-F., Nedelec, A., Martin, H., Jayananda, M. 2003. Syntectonic granite emplacement at different structural levels: the Closepet Granite, South India. Journal of Structural Geology 25, 611-631.

Mukherjee S, Ghosh G, Das K, Bose S, Hayasaka Y. 2017. Geochronological and geochemical signatures of the granitic rocks emplaced at the north -eastern fringe of the India: Implications for late Archean crustal growth. Geological Journal 1–21. https://doi.org/10.1002/gj.3007

Murthy, Y.G.K., BabuRao, Gupta Sarma, D., Rao, J.M., Rao, M.N and Bhattacharji,S. 1987. Tectonic, petrochemical and geophysical studies of mafic dyke swarms around the Proterozoic Cuddapah basin, south India. In: H.C. Halls and W.H. Fahrig,(Eds), Mafic dyke swarms. Geol.Assoc.Canada, Newfoundland, Canada, Spec. 34,. 303-316.

Naqvi, S.M., Rogers, J.J.W. 1987. Precambrian Geology of India. Oxford University Press, New York, N.Y., 223.

Pandey, B.K., Prasad, R.N.,Sastry, D.V.L.N., Kumar, B.R.M, SuryanarayanaRao,S. And Gupta, J.N. 1988. Rb-Sr whole rock ages for the granites from parts of Andhra Pradesh and Karnataka, In: Fourth national symposium on mass spectrometry, Indian Institute of sciences, Bangalore, India, EPS-3/1.

Pearce, J.A., Harris, N.B., Tindle, A.G. 1984. Trace element discrimination diagrams for the tectonic interpretation of granitic rocks. Journal of petrology 25, 956-983.

Peucat J-J, Jayananda M, Chardon D, Capdevila R, Fanning CM, Paquette J.L. 2013. The lower crust of the Dharwar Craton, south India: patchwork of Archean granulitic domains. Precambrian Research 227, 4-28.

Polat, A., Kerrich, R. 2001. Geodynamic processes, continental growth, and mantle evolution recorded in late Archean greenstone belts of the southern Superior Province, Canada. Precambrian Research 112, 5-25.

Polito, P.A., Kyser, T.K., Marlatt, J., Alexandre, P., Bajwah, Z., and Drever, G., 2004. Significance of alteration assemblages for the origin and evolution of the Proterozoic Nabarlek unconformity-related uranium deposit, NorthernTerritory, Australia: Economic Geology 99, 113−13

Rajaraman, H.S., NagendraBabu, G., Chavan, S.J., Achar, K.K., Ramesh Babu, P.V. 2013 Signature of Potassium Enrichment in Granite of the Chitrial Area, Nalgonda District, Andhra Pradesh: Inferences Using its U, Th, K2O, Na2O, Rb, Ba, and Sr Contents, Geol. Soc. India 82, 53-58.

Rudnick, R.L. 1995. Making continental crust. Nature 378, 571-577.

Santosh, M., Yang, Q.Y., Shaji, E., Tsunogae, T., Mohan, M.R., Satyanarayanan, M. 2015. An exotic Mesoarchean microcontinent: the Coorg Block, southern India. Gondwana Research, 27, 165-195.

Sharma, M., Rai, A.K., Nagabhusana, J.C., Sinha, R.M., Vasudeva Rao, M., 1995. Cuddapah Basin and its environs as first orger uranium target in the Proterozoic of India. Expln. Res. Atomic Minerals (AMD), 8, 127-139.

Sinha R.M., Shrivastava V.K., Sarma G.V.G. and Parthasarathy T.N. 1995. Geological favourability for unconformity related uraniumdeposits in northern parts of the Cuddapah Basin: evidences fromLambapur uranium occurrence, Andhra Pradesh, India. Exp. Res. At. Miner.,.8, 111–126.

Stacey, J.S. and Kramers, J.D. 1975. Approximation of Terrestrial Lead Isotope Evolution by a 2-Stage Model. Earth and Planetary Science Letters 26(2), 207-221.

Sundaram, S.M., Sinha, P.A., Ravindra Babu, B. and Muthu, V.T. 1989. Uranium mineralization in Vempalli Dolomite and Pulivendla conglomerate/ quartzite of Cuddapah basin, A.P. Indian Minerals, 43 (2), 98-103

Taylor, S.R., McLennan, S.M. 1995. The geochemical evolution of the continental crust. Reviews of Geophysics 33, 241-265.

Thomas, P.K., Thomas, T., Thomas, J., Pandian, M.S., Banerjee, R., Babu, P.R., Gupta, S. and Vimal, R., 2014. Role of hydrothermal activity in uranium mineralisation in Palnad Sub-basin, Cuddapah Basin, India. Journal of Asian Earth Sciences, 91, 280-288.

Umamaheswar, K., Achar, K. K. and Maithani, P.B. 2009. Proterozoic unconformity related uranium mineralisation in the Srisailam and Palnad sub-basins of Cuddapah Basin, Andhra Pradesh, India. IAEA–CN–175/28.

Verma, M.B., Som, A., Latha, A., Umamaheswar, K., Maithani, P.B. 2008. Geochemistry of host granitoids of uranium deposit at Chitrial area, Srisailam subbasin, Nalgonda District, Andhra Pradesh. Memoir of the Geological Society of India 73, 37-54.

Verma, M.B., Gupta, S., Singh, R.V., Latha, A., Maithani, P.B. and Chaki, A. 2009. Ore body characteristisation of Koppunuru uranium deposit in Palnadu sub-basin, Guntur district, Andhra Pradesh. Natl. Symp. on ‘Advances in Atomic Mineral Science in India during the 50 year period : 1959-2009’, Aug. 26-28, A.M.D., Hyderabad, Abstract, 51-52.

Whalen, J.B., Currie, K.L., Chappell, B.W. 1987. A-type granites: geochemical characteristics, discrimination and petrogenesis. Contributions to Mineralogy and Petrology 95, 407-419.

Table 1. A summary of location, Rock types, GPS co-ordinates, and obtained ages of the studied samples.

Sample	Rock type	GPS Location	Age (Ma.)
CT 206	Monzogranite	N16.598410° E79.003550°	2524±35 Ma
CT 220	Monzogranite	N16.561260° E79.089040°	2490±30 Ma
CT 210	Monzogranite	N16.497390° E79.051540°	2520±25 Ma
CT 31	Alkali-feldspar Granite	N16.473722° E79.003056°	2524±10Ma
CT 65	Monzogranite	N16.548778° E79.004472°	2525±24Ma
CT 62F	Monzogranite	N16.552472° E79.001972°	…….
CT 207A	Monzogranite	N16.526470° E79.020900°	2514±10 Ma
CT 214	Sandstone	N16.59785 E78.98413	2468±19 Ma
CT24	Sandstone	N16.51444 E79.03027	2488±18 Ma

Table.2 Stratigraphic succession of Chitrial area.

	Ore Mineralization	----------
Mesoproterozoic Srisailam Sediments	Ferruginous quartzite Shale and quartzite intercalations Conglomerate / Pebbly Quartzite 1-3 m with thin black layers of grey shale .....Nonconformity.....	*ca*. 1.7 Ga (U-Pb Zircon) (Collins et al.,2015)
	Dolerite Dyke	????
Archean to Paleoproterozoic	Basement Granite	*ca*. 2.51 Ga - *ca*. 2.52 Ga (U-Pb Zircon) (Mukherjee et al., 2017)

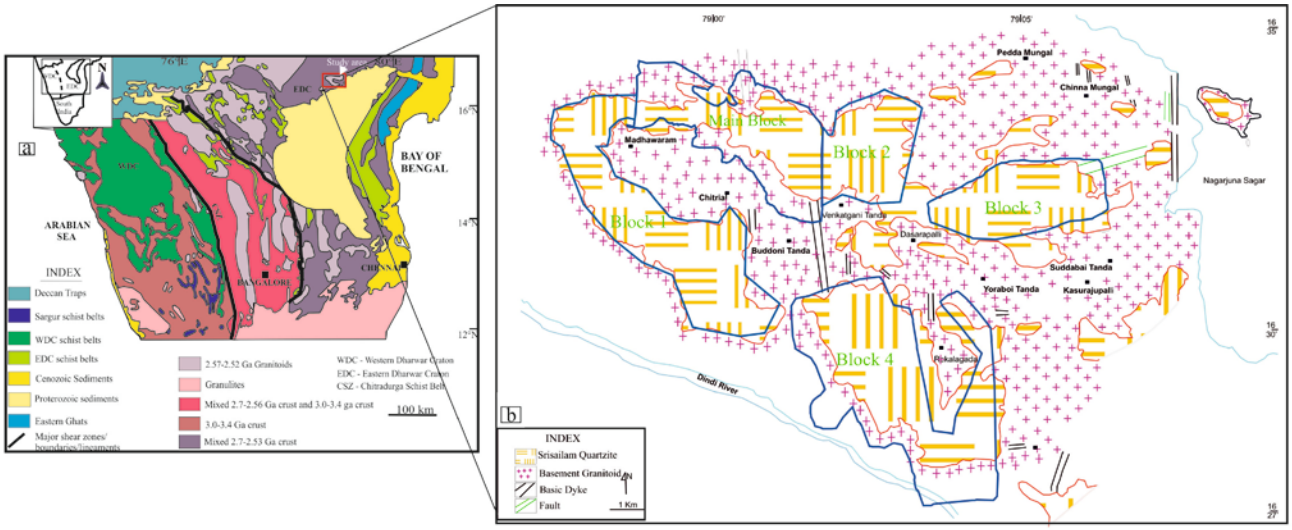

Fig. 1: (a)Detailed geological map of Dharwar Craton (modified after Jayananda et al., 2014). Inset shows the position of Dharwar craton within India. Position of Chitrial outlier is marked by the red rectangle. (b) Lithological map of Chitrial area.

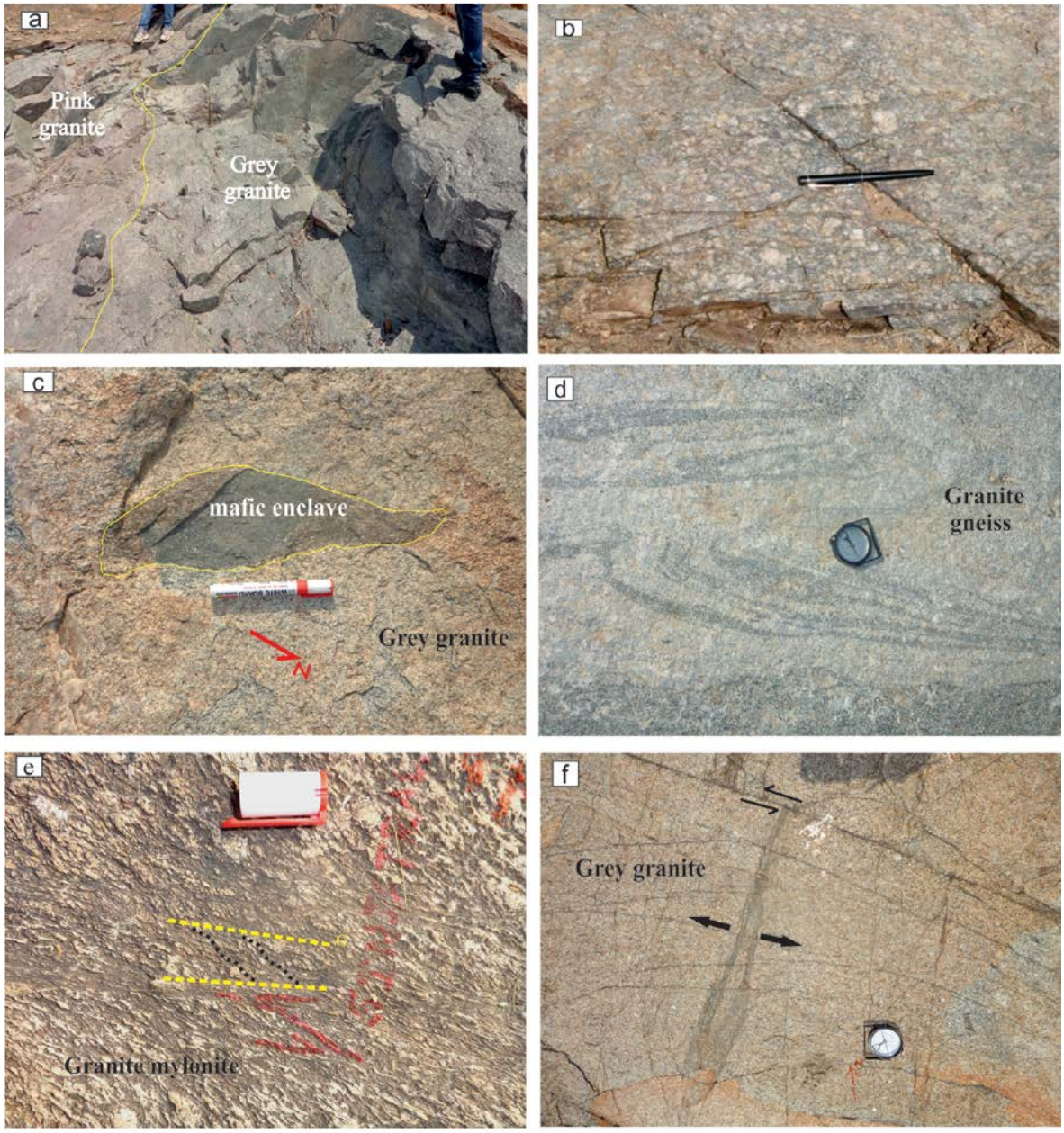

Fig. 2: Field photograph a) gradual change of grey granite to pink granite, b)Porphyritic granite, c) elliptical and stretched mafic enclaves within granite, (d) gneissic layering within granite, e) gneissic fabric changes to a mylonitic fabric with sinistral slip sense, yellow line denotes the gneissic foliation, f) A late brittle deformation affects the basement rocks and both shear and mixed-mode fractures of variable orientations develop.

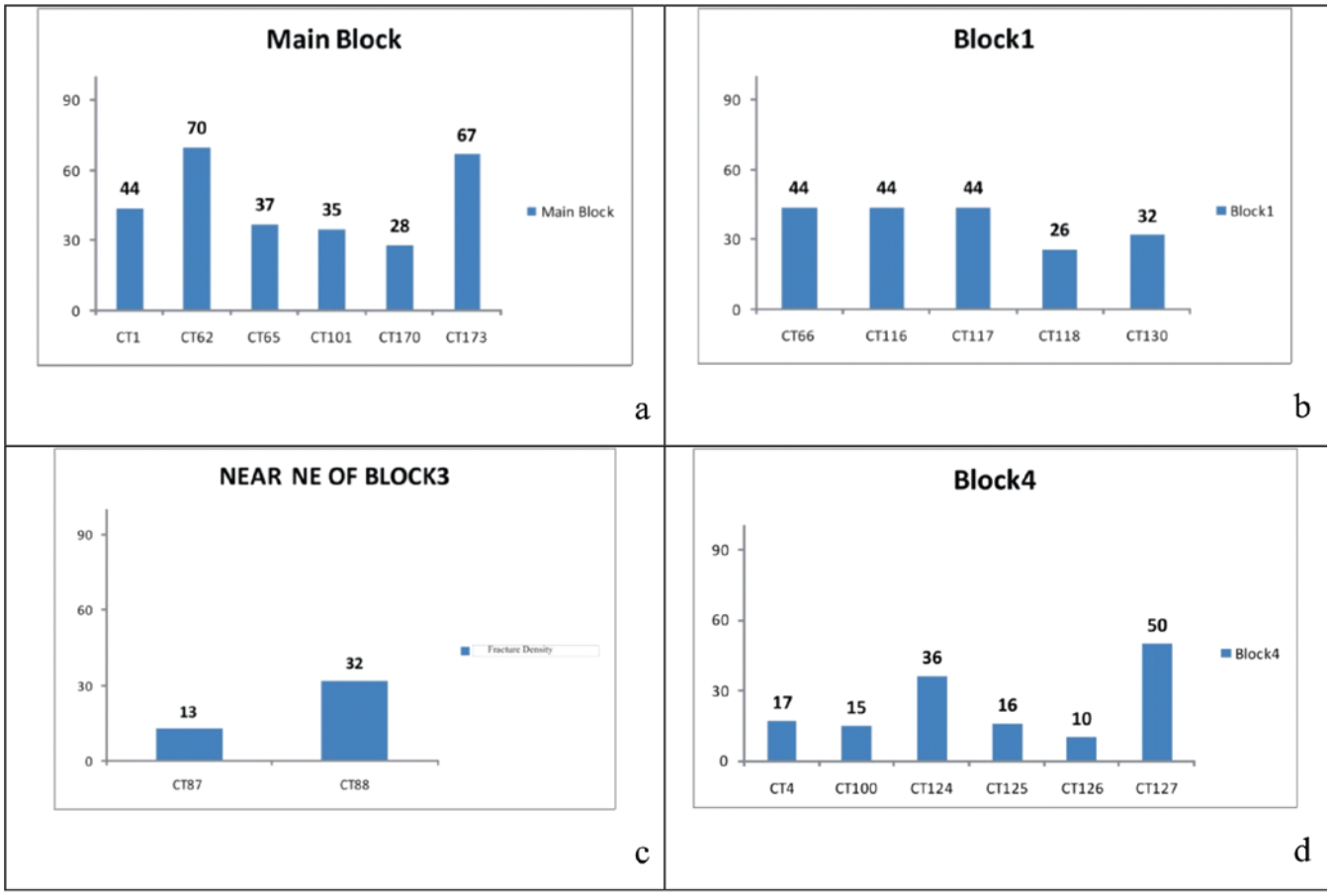

Fig.3: Block wise histogram diagram of fracture density showing fracture maximum intensity in Main Block.

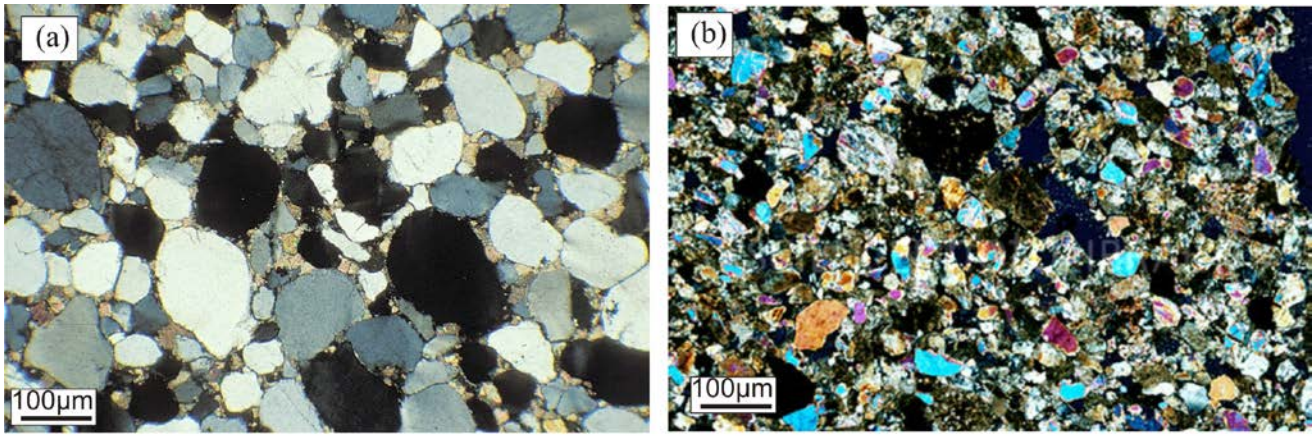

Fig.4: a) Framework mainly constitute of quartz. b) Feldspar show corroded grain margin.

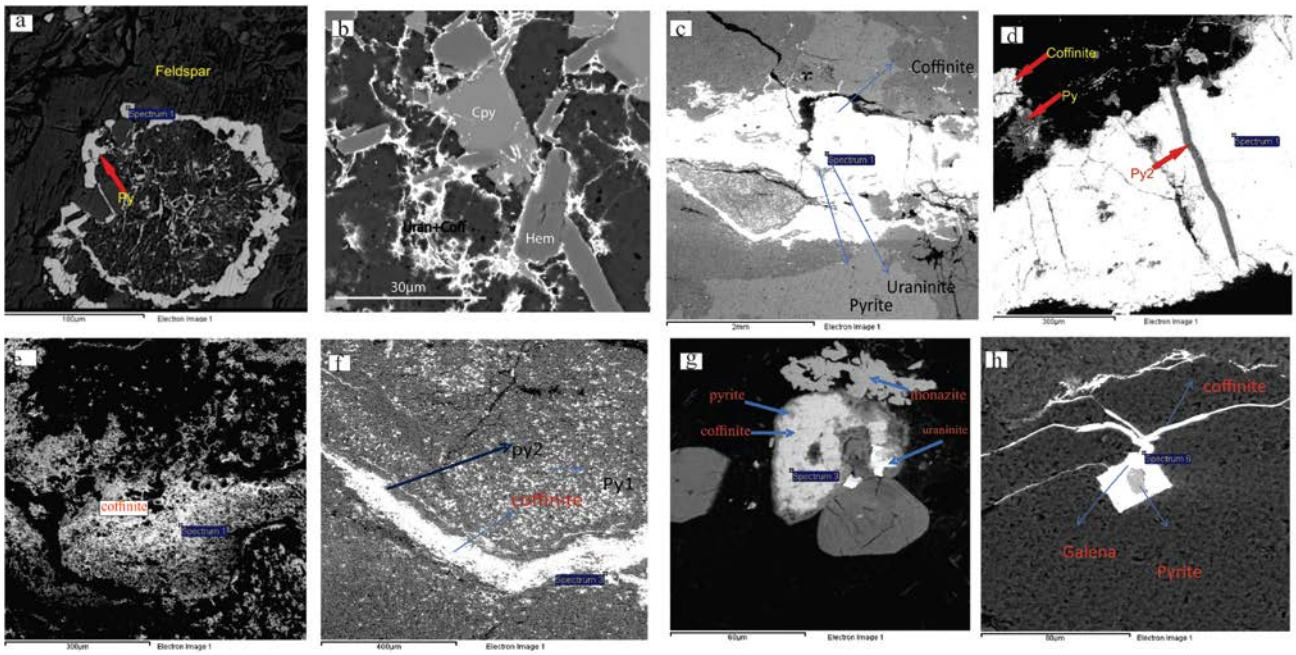

Fig. 5: BSE images of mineralization presents within basement granites. (a) Pyrite present as a rim around feldspar. (b) Hematite occurs crosscutting chalcopyrite. c) Veins cemented by uraninite and coffinite. d) Pyrite veins crosscut the uranium bearing vein. e) Colloform texture of coffinite. f) Coffinite presents along fracture. g) Uraninite alters to coffinite. h) Galena presents as a rim around pyrite.

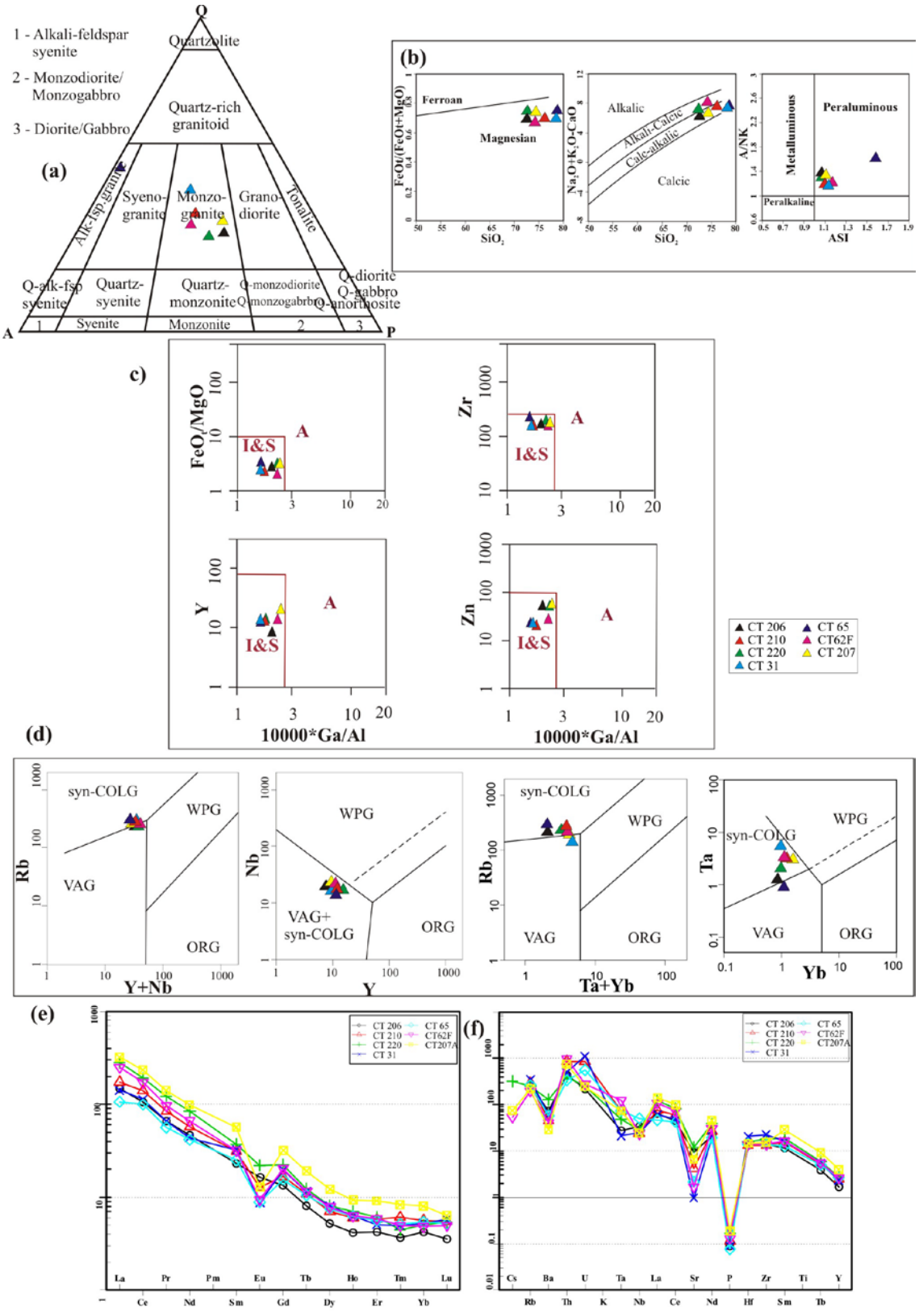

Fig.6: a) QAPF diagram showing six samples plot within monzogranite field and one sample within the alkali-feldspar granite field. b) Plot of all the samples within discrimination diagram (Frost et al., 2001) shows magnesian and peraluminous characte. c) Multiple plots involving trace elements and REE of the samples: FeO/Mgo vs. Ga/Al, Zr vs. Ga/Al, Y vs. Ga/Al, and Zn vs. Ga/Al, (Whalen, 1987). (d) Tectonic discrimination plot of Rb vs. (Y+Nb), Nb vs. Y, Rb vs. (Ta+Yb), Ta vs. Yb (Pearce et al., 1984). e) Chondrite-normalized REE plots (Boynton, 1984) of the samples. f) Primordial mantle-normalized REE plots (Taylor and McLennan, 1995) of the same samples.

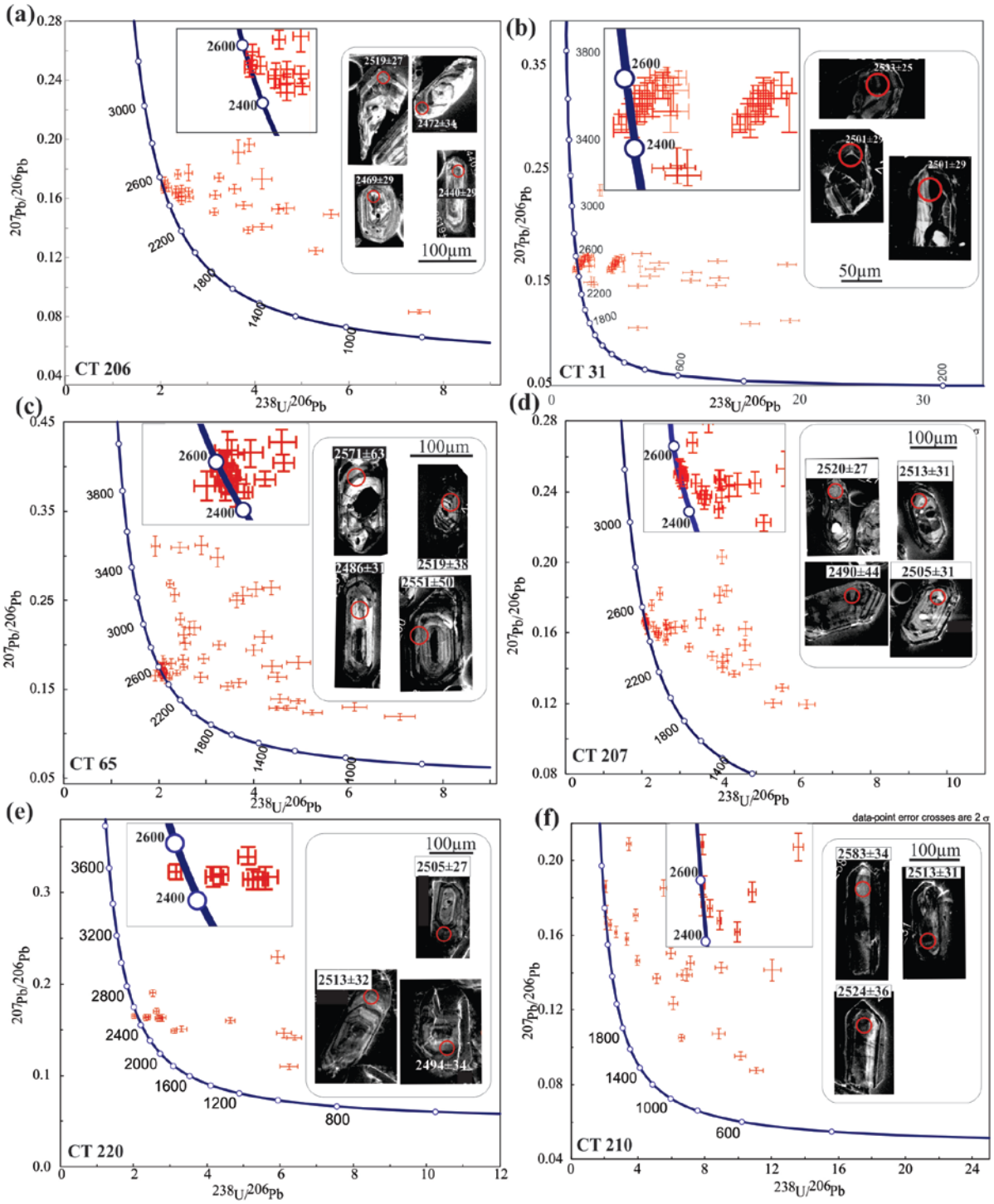

Fig.7: (a) Plot of zircon U-Pb spot data of sample CT206 in Terra-Wasserburg diagram (n=31). Inset shows representative zircon grains.(b) Plot of zircon U-Pb data of sample CT31 in Terra-Wasserburg diagram (n=34). Representative zircon CL images in the inset show masking of faint traces of planar or oscillatory zoning. (c) Plot of zircon U-Pb spot data of sample CT65 in Terra-Wasserburg diagram (n=61). Zircon grains in the inset show presence of dark-CL xenocrystic cores having traces of fine-scale oscillatory zoning. (d) Plot of zircon U-Pb spot data of sample CT207 in the Terra-Wasserburg diagram for sample CT 207 (n=43). Zircon grains inthe inset show weak oscillatory zoning surrounding dark-CL xenocrystic cores. (e) Zircon U-Pb data of sample CT220 plotted in the Terra-Wasserburg diagram (n=43). Inset shows CL images of neoblastic zircon grains. (f) Zircon U-Pb data of sample CT210 in Terra-Wasserburg diagram (n=23). Representative zircon grains in the inset.

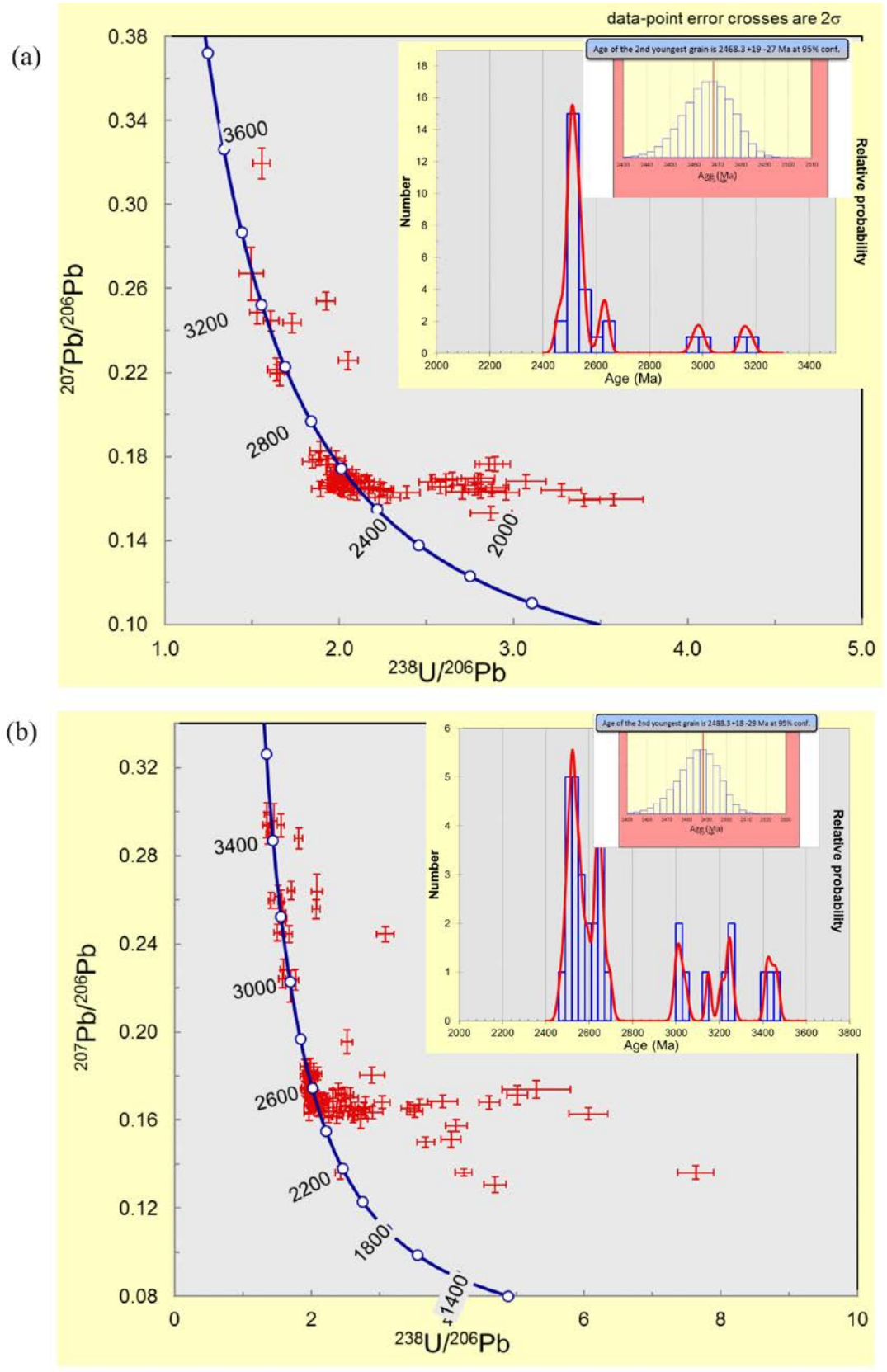

Fig.8: a) Plot of detrital zircon U-Pb spot data of sample CT214 in Terra-Wasserburg diagram (n=78).
b) Plot of detrital zircon U-Pb spot data of sample CT24 in Terra-Wasserburg diagram (n=99).

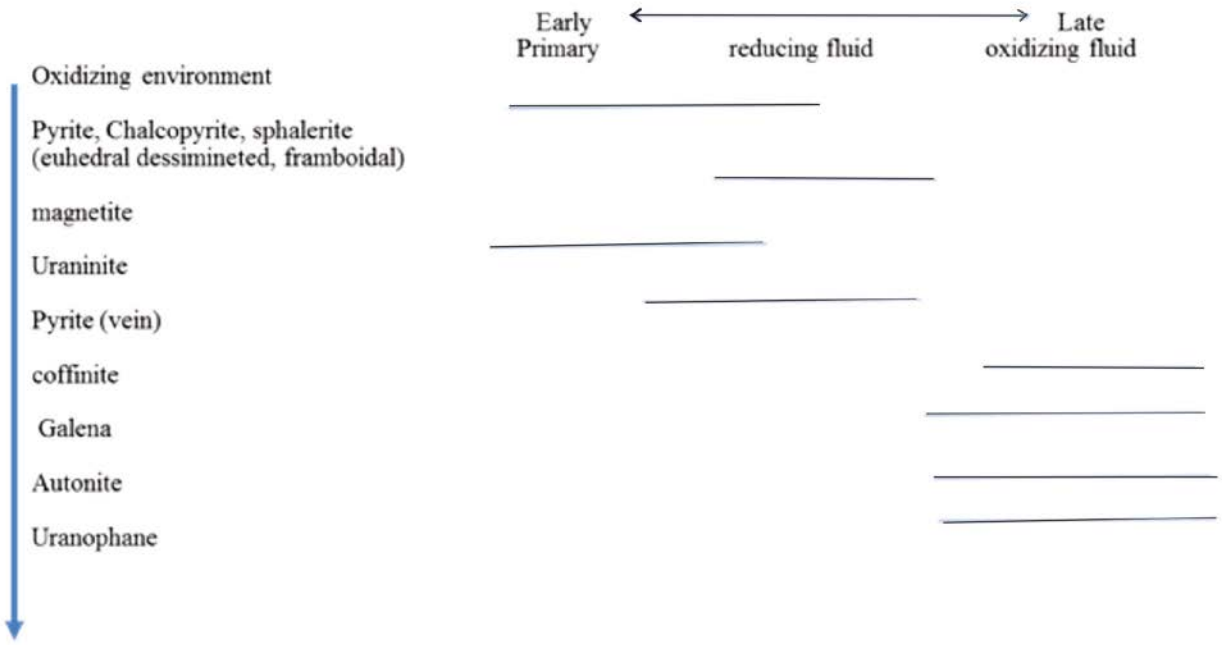

Fig. 9: Paragenetic history of mineralization presents within basement granites

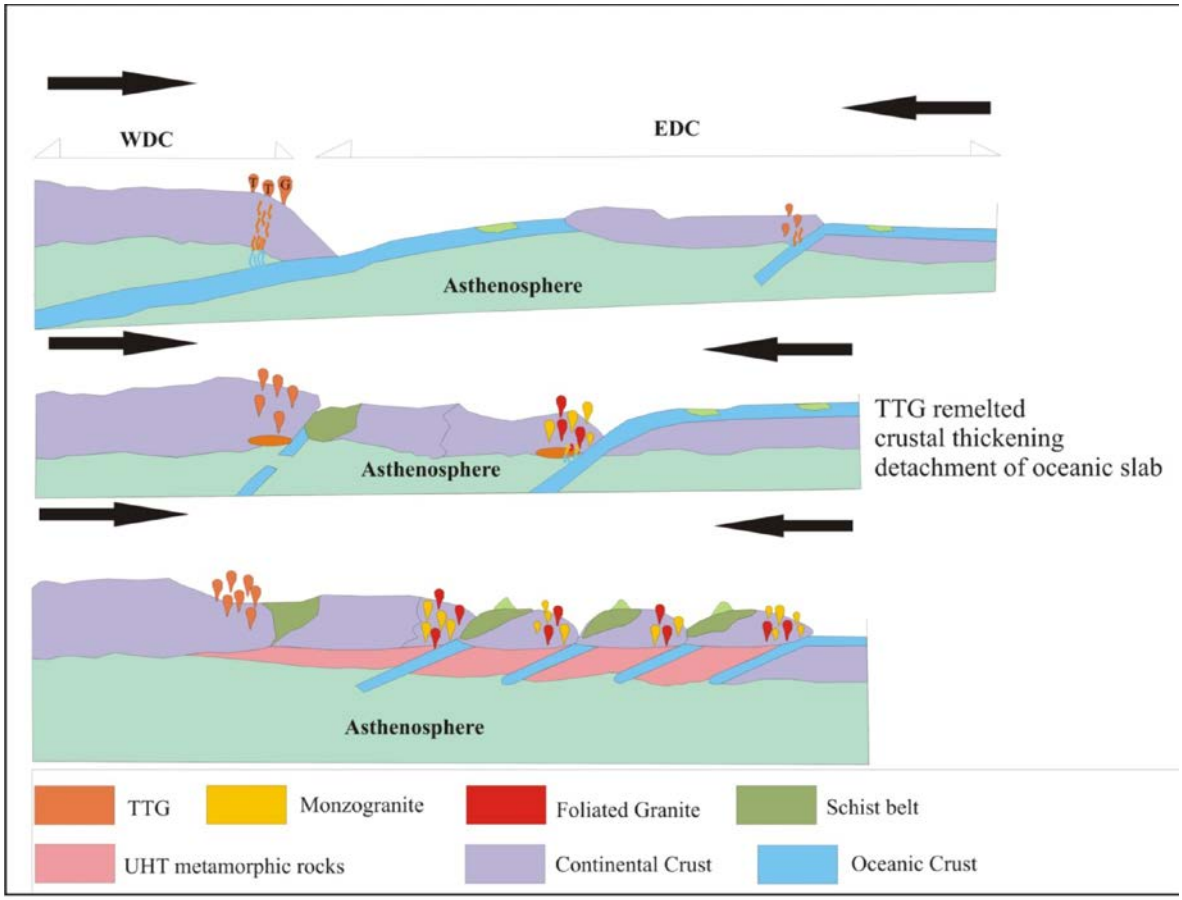

Fig.10: Schematic diagram represents the geodynamic evolution and formation of monzogranite